

# Selective Alkane C–H Bond Oxidation Catalyzed by a Non-Heme Iron Complex Featuring a Robust Tetradentate Ligand

Lizhu Chen,<sup>1</sup> Xiao-Jun Su,<sup>1</sup> and Jonah W. Jurss<sup>1\*</sup>

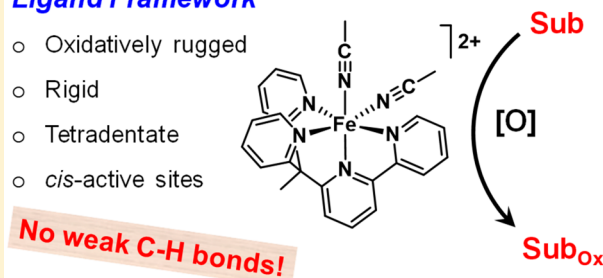
Department of Chemistry and Biochemistry, University of Mississippi, University, Mississippi 38677, United States

## Supporting Information

**ABSTRACT:** An iron complex,  $[\text{Fe}^{\text{II}}(\text{BpyPY2Me})(\text{CH}_3\text{CN})_2](\text{OTf})_2$  (1-Fe, where BpyPY2Me is 6-(1,1-di(pyridin-2-yl)ethyl)-2,2'-bipyridine and OTf is triflate), supported by an oxidatively rugged tetradentate ligand is reported for the catalytic oxidation of unactivated C–H bonds in cyclohexane and adamantane. With the use of *m*-chloroperbenzoic acid (*m*CPBA) as the terminal oxidant, the iron catalyst shows an alcohol-to-ketone (A/K) ratio of 7.5 for cyclohexane oxidation with conversion percentages as high as 90% with respect to oxidant. Moreover, catalysis toward adamantane oxidation shows high regioselectivity ( $3^\circ/2^\circ = 45$ ) favoring tertiary C–H bonds with yields up to 87%. Results, including electrospray ionization mass spectrometry and UV–vis spectroscopy, indicate that a molecular non-heme iron(IV)-oxo intermediate is the catalytically active species.

### Ligand Framework

- Oxidatively rugged
- Rigid
- Tetradentate
- *cis*-active sites



Raw chemical feedstocks, such as petroleum and natural gas, are important sources of inexpensive hydrocarbons for the chemical and pharmaceutical industries. However, they have thermodynamically stable, kinetically inert C–H bonds that are not often viewed as chemical handles for further manipulation. A challenge lies in converting these readily available feedstocks into versatile organic building blocks in a mild and atom economical manner.<sup>1</sup> In this context, synthetic iron-oxo catalysts have been developed for reactions such as olefin epoxidation<sup>2–4</sup> and the hydroxylation of unactivated C–H bonds.<sup>5–7</sup> Circuitous synthetic routes engrossed in the maintenance and interconversion of functional groups throughout a reaction sequence can be avoided with catalysts capable of selective C–H bond functionalization.<sup>7</sup> Despite the remarkable progress that has been made to demonstrate the scope of chemistry available to synthetic non-heme iron-oxo catalysts,<sup>5</sup> significant improvements in catalyst selectivity and stability are needed to realize the full potential of these systems.<sup>8</sup>

Notably, iron-oxo complexes are capable of catalyzing *N*-dealkylation reactions,<sup>9</sup> which has particular relevance to catalyst stability as the majority of non-heme Fe-oxo catalysts employ alkylamine-type ligands. Prominent iron-based catalysts of this ilk are shown in Figure 1. Amine-based ligands are convenient to synthesize by  $\text{S}_{\text{N}}2$  reactions but are vulnerable to oxidative decomposition.<sup>9,10</sup> Likewise, C–H bonds of the ligand can also be oxidized through both inter- and intramolecular pathways.<sup>10,11</sup> Demetalation and individual donor dissociation from iron have also been observed with the flexible, polydentate ligands that are commonly used.<sup>12,13</sup>

Beyond stability, metal coordination geometry is another important factor as many of the champion iron catalysts applied to hydrocarbon oxidation feature *cis*-labile coordina-

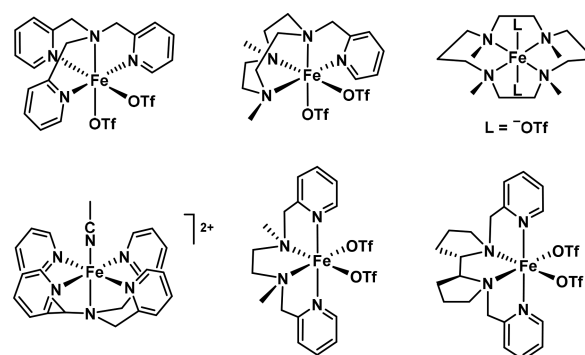


**Figure 1.** Representative non-heme iron complexes for C–H bond oxidation bearing alkylamine-type N-donor ligands.

tion sites.<sup>14</sup> The increased activity and selectivity observed with these catalysts is thought to arise from cooperativity between the adjacent sites as proposed in water- or acetic-acid-assisted mechanisms for alkane oxidation.<sup>7,15</sup> It is worth noting that non-heme iron oxygenases also possess this structural motif.<sup>15</sup> While the protein environment around metalloenzyme active sites serves, in part, to protect the active site from degradation, synthetic catalysts do not have the luxury of a tightly controlled surrounding and must be designed to withstand the harsh oxidizing conditions of the reaction medium. Thus, we have turned our attention toward more rigid, pre-organized frameworks devoid of weak C–H bonds and alkylamine-type donors as a starting point to enforcing

**Received:** August 25, 2018

desired active site configurations and improved catalyst stability.

Herein, we report an iron(II) complex,  $[\text{Fe}^{\text{II}}(\text{BpyPY2Me})(\text{CH}_3\text{CN})_2](\text{OTf})_2$  (**1-Fe**, where BpyPY2Me is 6-(1,1-di(pyridin-2-yl)ethyl)-2,2'-bipyridine and OTf is triflate), supported by an oxidatively rugged tetradentate scaffold that aims to minimize oxidative ligand decomposition while providing *cis*-labile coordination sites at the iron center. Literature procedures were followed to prepare BpyPY2Me.<sup>16</sup> Complex **1-Fe** was prepared by reacting BpyPY2Me with 1 equiv of  $\text{Fe}(\text{OTf})_2$  in methanol. The complex was subsequently crystallized from acetonitrile by diethyl ether diffusion and structurally characterized (Figure 2) by single-

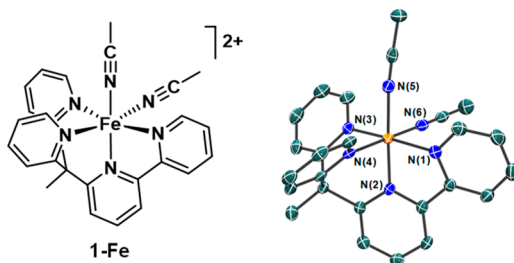


**Figure 2.** Crystal structure of the cation of  $[\text{1-Fe}](\text{OTf})_2$  with thermal ellipsoids rendered at the 70% probability level. Hydrogen atoms have been omitted for clarity. Selected bond distances: Fe–N(1), 1.9948(19); Fe–N(2), 1.9054(19); Fe–N(3), 1.9691(19); Fe–N(4), 1.9509(19); Fe–N(5), 1.951(2); Fe–N(6), 1.950(2) Å.

crystal X-ray crystallography. Selected bond lengths, provided in the caption, and the diamagnetic  $^1\text{H}$  and  $^{13}\text{C}$  nuclear magnetic resonance (NMR) spectra of **1-Fe** are consistent with a low-spin iron(II) complex (Figures S1 and S2).

With the addition of one equivalent (equiv) of *m*-chloroperbenzoic acid (*m*CPBA) into the  $\text{CH}_3\text{CN}$  solution containing 1 mM **1-Fe**, the initial absorption at  $\lambda = 486$  nm ( $\epsilon = 2700 \text{ M}^{-1} \text{ cm}^{-1}$ ) gives way to a new broad absorption band centered at 739 nm ( $\epsilon \approx 100 \text{ M}^{-1} \text{ cm}^{-1}$ ), a characteristic absorption feature of known Fe-oxo complexes (Figure 3).<sup>17</sup>

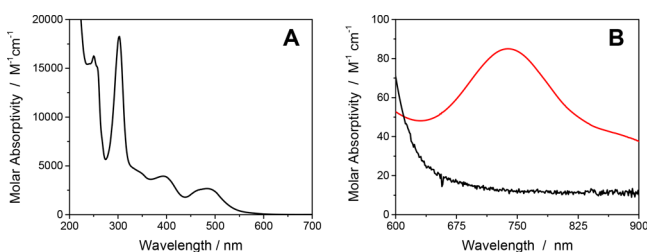


**Figure 3.** UV-vis spectra of (A) **1-Fe** (black) in anhydrous acetonitrile [ $\lambda_{\text{max}} = 250$  nm ( $\epsilon = 1.6 \times 10^4 \text{ M}^{-1} \text{ cm}^{-1}$ ), 302 nm ( $1.8 \times 10^4 \text{ M}^{-1} \text{ cm}^{-1}$ ), 395 nm ( $3.9 \times 10^3 \text{ M}^{-1} \text{ cm}^{-1}$ ), and 486 nm ( $2.7 \times 10^3 \text{ M}^{-1} \text{ cm}^{-1}$ )] and (B) the iron(IV)-oxo intermediate (red) formed by adding 1 equiv of *m*CPBA.

High-resolution electrospray ionization mass spectrometry (ESI-MS) confirmed its identity as a high-valent, molecular iron(IV)-oxo species (Figure S3). A paramagnetic  $^1\text{H}$  NMR spectrum was also obtained of the iron-oxo complex with proton signals spanning a range of 54 ppm (Figure S4). This intermediate is relatively stable ( $t_{1/2} \sim 30$  min at 23 °C; Figures S5, S6) when monitoring self-degradation by the decrease in absorbance at 739 nm. We note that  $\text{H}_2\text{O}_2$  addition

to solutions of **1-Fe** did not generate the near-infrared absorption band, which suggests that  $\text{H}_2\text{O}_2$  is not a strong enough oxidant to form an iron-oxo species from **1-Fe**.

Cyclic voltammetry (CV) of **1-Fe** was performed in  $\text{CH}_3\text{CN}$  solutions containing 0.1 M  $\text{LiClO}_4$  as the supporting electrolyte (Figure S7). All reported potentials are referenced to the ferrocenium/ferrocene couple ( $\text{Fc}^{+/0}$ ). In anhydrous  $\text{CH}_3\text{CN}$ , **1-Fe** undergoes a reversible ( $\Delta E_p = 69$  mV) one-electron redox process at  $E_{1/2} = 0.89$  V, consistent with an  $\text{Fe}^{\text{III}}(\text{CH}_3\text{CN})_2/\text{Fe}^{\text{II}}(\text{CH}_3\text{CN})_2$  couple. No additional waves were observed when scanning to more positive voltages. At negative potentials, two quasi-reversible, overlapping reductions are found at  $E_{p,c} = -1.66$  and  $-1.83$  V, which we assign to ligand-based reductions based on the CV of a reported Zn(II) complex bearing a very similar ligand that exhibits two closely spaced reductions at similar potentials.<sup>18</sup>

Because **1-Fe** can be oxidized with *m*CPBA to generate an iron-oxo complex, its application as a catalyst for cyclohexane C–H bond oxidation was investigated (Figure S8). The ratio of cyclohexanol-to-cyclohexanone, i.e., the alcohol-to-ketone ratio (A/K), has been used to differentiate between a likely radical-based mechanism or a metal-centered oxidation process.<sup>1</sup> The so-called radical mechanism typically proceeds through a long-lived radical formed via Fenton-type chemistry in which the oxidant, i.e., peroxide, is decomposed into radicals that oxidize the substrate directly. In this case, the cyclohexyl radical is susceptible to reactivity with  $\text{O}_2$  to form cyclohexyl peroxide, which exhibits low selectivity in decomposing to equivalent amounts of cyclohexanol and cyclohexanone (with an A/K ratio of  $\sim 1$ ). However, metal-centered C–H bond oxidations are often characterized by short radical lifetimes that allow higher A/K product ratios and greater selectivity.<sup>1</sup> Here, a transient substrate radical is formed by H atom abstraction by the Fe-oxo catalyst and rebounds with the resulting Fe–OH species to form the C–O bond of the product.

All reactions were conducted in  $\text{CH}_3\text{CN}$  at room temperature with a large excess of substrate to avoid overoxidation of cyclohexanol (A) to cyclohexanone (K). Catalytic reactions were repeated in triplicate, and products were quantified by gas chromatography. The conversion percentages with respect to oxidant, taking the reaction stoichiometry into account ( $\text{A} + 2\text{K}$ ), are presented in Table 1. The results show that

**Table 1.** Cyclohexane Oxidation with *m*CPBA Catalyzed by **1-Fe**<sup>a</sup>

entry	1-Fe/ <i>m</i> CPBA/substrate		
		A/K <sup>b</sup>	overall yield (%) <sup>c</sup>
1	1:10:100	2.5	48
2	1:10:500	5.6	79
3	1:10:800	5.8	80
4	1:10:1000	7.5	90
5	1:20:100	1.4	48
6	1:20:500	3.8	78
7	1:20:800	3.9	80
8	1:20:1000	4.8	84

<sup>a</sup>Conditions: 1 mM **1-Fe**, 3 mL total volume. <sup>b</sup>Ratio of moles of cyclohexanol to moles of cyclohexanone. <sup>c</sup>Yield with respect to *m*CPBA.

cyclohexanol is the main product for all entries. When 10 equiv of *m*CPBA and 1000 equiv of cyclohexane are used, the highest conversion yield of 90% and largest A/K ratio (7.5) are observed, consistent with a metal-centered oxidation mechanism.<sup>1</sup> A small increase in the A/K ratio to 9 was observed in experiments conducted in the absence of O<sub>2</sub>. In addition, a series of reactions were quenched with triphenylphosphine at different time points following the addition of *m*CPBA to measure the A/K ratio as a function of time. The A/K ratios are largely unaffected by the reaction time (Figure S9).

Reaction kinetics for cyclohexane oxidation were also analyzed by monitoring the decay of the preformed Fe(IV)-oxo intermediate upon addition of different amounts of substrate (Figure S10). Pseudo-first-order rate constants ( $k_{\text{obs}}$ ) were determined by fitting the kinetic traces and were found to increase linearly with increasing cyclohexane concentration (Figure S11). From the slope of this plot, a second-order rate constant ( $k_2$ ) of  $1.4 \times 10^{-2} \text{ M}^{-1} \text{ s}^{-1}$  at 23 °C was obtained. Using various ratios of cyclohexane to *d*<sub>12</sub>-cyclohexane (Figure S12), a kinetic isotope effect (KIE) of 3.2 was calculated (Figure S13) in experiments carried out under the same conditions as entry 4 of Table 1. The KIE value as well as the A/K ratios measured with 1-Fe are similar to reported values for known non-heme iron-oxo complexes.<sup>14a</sup>

To address one of the primary aims of this work, the catalytic stability of 1-Fe was also investigated by analyzing the amount of oxidized product relative to the amount of added *m*CPBA. Here, *m*CPBA (10 equiv) was added every 10 min into a CH<sub>3</sub>CN solution containing 1 mM 1-Fe and 1000 equiv of cyclohexane. As shown in Figure 4, the total amount of

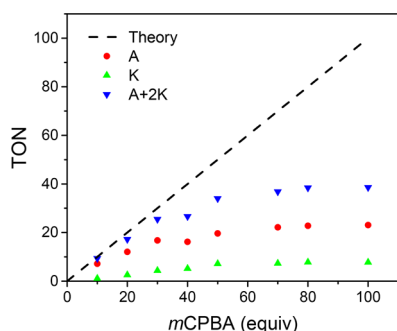


**Figure 4.** Plot of turnover number (TON), moles of product/moles of catalyst, for each product versus equivalents of added *m*CPBA oxidant to 1 mM 1-Fe and 1000 equivalents of cyclohexane in CH<sub>3</sub>CN. The theoretical maximum TON for cyclohexane is shown with the dashed line, and the A+2K values reflect total consumption of *m*CPBA to generate products as two equivalents of *m*CPBA are required to form cyclohexanone from cyclohexane.

oxidized product (A + 2K) is close to the theoretical value up to 30 equiv of *m*CPBA. At 100 total equivalents of *m*CPBA, the yield of oxidized products approaches 40%. A comparable conversion of 48% is observed with the same ratio of *m*CPBA to cyclohexane where the oxidant was added all at once (Table 1, entry 1). These results are consistent with slow deactivation of 1-Fe. When the added oxidant totals 50 equiv, conversion to both cyclohexanol and cyclohexanone approaches a plateau, indicating almost complete deactivation of the catalyst after 5 cycles of added *m*CPBA (10 equiv/cycle). After 5 cycles, overall conversion is 70% with an alcohol-to-ketone ratio of 2.7 and a total turnover number (TON) of 35.

Encouraged by these results, the catalytic oxidation of adamantane (Figure S14) was investigated to assess the ability of 1-Fe to select between its tertiary and secondary C–H bonds, which have reported bond dissociation energies of 96.2 and 100.2 kcal/mol, respectively.<sup>19</sup> Adding 10 equiv of *m*CPBA into CH<sub>3</sub>CN solutions containing 1 mM 1-Fe and 10 equiv of adamantane gives an 87% conversion yield with a regioselectivity ratio of 45 for tertiary sites (3°) to secondary sites (2°). Compared with other molecular iron-oxo catalysts, 1-Fe exhibits high selectivity for tertiary C–H bonds in adamantane oxidation with high conversion (Table 2).

**Table 2.** Comparison of Selected Iron Catalysts for Adamantane Oxidation

catalysts <sup>a</sup>	oxidant	3°/2° <sup>b</sup>	yield (%) <sup>c</sup>	ref
1-Fe	<i>m</i> CPBA	45	87	this work
Fe <sup>III</sup> TPPCL	PhIO	48	14	20
2	<i>m</i> CPBA	110	29	21
3	H <sub>2</sub> O <sub>2</sub>	30	19	22
4	H <sub>2</sub> O <sub>2</sub>	25	31 <sup>d</sup>	23
5	H <sub>2</sub> O <sub>2</sub>	28	–	24
6	H <sub>2</sub> O <sub>2</sub>	33	–	14a
7	<i>m</i> CPBA	17	50 <sup>d</sup>	25

<sup>a</sup>Catalyst structures are shown in Figure S16. <sup>b</sup>3°/2° =  $3 \times [1\text{-adamantanol}/(2\text{-adamantanol} + 2\text{-adamantanone})]$ . <sup>c</sup>Yield with respect to oxidant. <sup>d</sup>Calculated from data provided in the cited work.

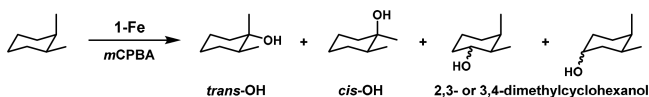
Moreover, with increasing amounts of *m*CPBA added to 500 equiv of adamantane and 1 mM 1-Fe, selectivity remains unchanged even as overall conversion begins to plateau around 50% at higher oxidant-to-substrate ratios (Figure S15). Importantly, control experiments for both cyclohexane and adamantane oxidation were conducted under the same conditions but in the absence of catalyst; no conversion to products was observed after 2 h from direct substrate oxidation by *m*CPBA.

The selected iron complexes, summarized in Table 2 and shown in Figure S16, have some of the highest reported 3°/2° values for the regioselective oxidation of adamantane. Until recently, the highest selectivity for the tertiary C–H bond sites of adamantane was observed with an iron porphyrin-based catalyst (Fe<sup>III</sup>TPPCL).<sup>20</sup> In 2017, Gupta and co-workers developed a more robust, nitro-substituted biuret-modified tetra-amido macrocycle (bTAML) to obtain iron catalyst 2 with remarkable regioselectivity (3°/2° of 110), albeit with a 29% yield.<sup>21</sup> Notably, the unsubstituted Fe-bTAML catalyst produced a 3°/2° product ratio of 69 and a conversion yield of just ~2%, highlighting the importance of catalyst stability.<sup>21</sup> Indeed, 1-Fe has comparable selectivity to Fe<sup>III</sup>TPPCL but with 6-fold higher conversion at 87%. In contrast to the macrocyclic examples, catalysts 3 through 6 of Table 2 and 1-Fe possess *cis*-labile coordination sites.<sup>14a,22–24</sup> Relative to these systems, 1-Fe exhibits superior selectivity for adamantane tertiary C–H bonds and, to the best of our knowledge, affords the highest yield with respect to oxidant of all reported iron complexes for adamantane oxidation. The high regioselectivities obtained with 1-Fe and macrocycles Fe<sup>III</sup>TPPCL and 2 also suggest that the relative orientation of open coordination sites is less important than other factors in this reaction. Catalyst 7 is a dinuclear iron complex with two metal center active sites, which may account for its relatively high conversion yield of 50%.<sup>25</sup>



Next, the oxidation of *cis*-dimethylcyclohexane was examined to assess the ability of **1-Fe** to catalyze the stereospecific hydroxylation of its tertiary C–H bonds. Results summarizing the reactivity and stereoselectivity of **1-Fe** are given in Table 3.

**Table 3. Regioselective Oxidation of *cis*-Dimethylcyclohexane**



entry	1-Fe/substrate/ <i>m</i> CPBA/ AcOH	conversion (%) <sup>a</sup>	RC (%) <sup>b</sup>	selectivity (%) <sup>c</sup>
1	1:25:10	72	100	66
2	1:25:20	54	100	77
3	1:120:100	25	90	72
4	1:120:100:0.5	21	90	71

<sup>a</sup>Conversion efficiency with respect to *m*CPBA. <sup>b</sup>Retention of configuration, RC = [(*trans*-OH – *cis*-OH)/(*trans*-OH + *cis*-OH)] × 100. <sup>c</sup>Overall selectivity for *trans*-OH = [*trans*-OH/(*trans*-OH + *cis*-OH + 2,3-OH + 3,4-OH)] × 100.

The degree to which stereoinformation is retained in the oxidation products also reports on the lifetime of alkyl radicals formed during the reaction.<sup>26</sup> Hydroxylation of the tertiary C–H bonds can occur with retention or inversion of configuration, which reflects the competition between C–O bond formation and epimerization of the tertiary alkyl radical intermediate. Very short radical lifetimes result in high stereospecificity, in which C–O bond formation is fast and the original configuration is preserved to yield *trans*-1,2-dimethylcyclohexanol (in which the methyl groups are *cis* to one another).<sup>14a</sup> In contrast, long-lived radicals should result in nearly equivalent amounts of *cis* and *trans* tertiary alcohol products.<sup>26</sup> With **1-Fe**, 100% retention of configuration (RC) is observed following the addition of 10 or 20 equiv of *m*CPBA to 25 equiv of *cis*-dimethylcyclohexane substrate (entries 1 and 2, Figure S17). Accounting for the small amount of 2,3- and 3,4-dimethylcyclohexanol produced (2,3-OH and 3,4-OH, respectively), the regioselectivity for *trans*-OH is also as high as 77%. Only a minor loss in stereoretention is observed at lower catalyst loading (entry 3, Figure S18), albeit with a drop in overall conversion. The addition of 0.5 equiv of acetic acid has previously been shown to improve conversion and selectivity for C–H bond oxidation with a non-heme iron catalyst;<sup>7</sup> however, there was no improvement with **1-Fe** in the presence of acetic acid (entry 4).

In closing, we have developed a new Fe(II) complex supported by a robust polypyridine ligand that engenders *cis*-labile coordination sites at iron. Using *m*CPBA as the terminal oxidant, we studied the catalytic activity of **1-Fe** in the functionalization of non-activated alkane C–H bonds with bond dissociation energies as high as 100 kcal/mol. Results from ESI-MS and UV–vis spectroscopy indicate that a molecular iron(IV)-oxo species is generated as the catalytically active species. The observed selectivity in cyclohexane and adamantane oxidation are consistent with a catalytic process mediated by a metal-centered oxidant rather than hydroxyl radicals. Several key observations demonstrate the high selectivity exhibited by **1-Fe**, which include high alcohol-to-ketone ratios in cyclohexane oxidation, the stereospecific hydroxylation of *cis*-1,2-dimethylcyclohexane, and the strong preference for tertiary C–H bonds in adamantane. The 3°/2°

selectivity ratio of 45 for adamantane oxidation is among the highest reported for molecular iron-oxo catalysts. Moreover, high conversion yields with respect to oxidant attest to the improved stability of this iron catalyst in hydrocarbon oxygenation.

## ■ ASSOCIATED CONTENT

### Supporting Information

The Supporting Information is available free of charge on the ACS Publications website at DOI: 10.1021/acs.organomet.8b00611.

Materials and methods, synthetic procedures, characterization, X-ray crystallographic data, A/K ratios vs time, reaction kinetics, KIE plot, and representative gas chromatograms (PDF)

### Accession Codes

CCDC 1863860 contains the supplementary crystallographic data for this paper. These data can be obtained free of charge via [www.ccdc.cam.ac.uk/data\\_request/cif](http://www.ccdc.cam.ac.uk/data_request/cif), or by emailing [data\\_request@ccdc.cam.ac.uk](mailto:data_request@ccdc.cam.ac.uk), or by contacting The Cambridge Crystallographic Data Centre, 12 Union Road, Cambridge CB2 1EZ, UK; fax: +44 1223 336033.

## ■ AUTHOR INFORMATION

### Corresponding Author

\*E-mail: [jwjurss@olemiss.edu](mailto:jwjurss@olemiss.edu).

### ORCID

Lizhu Chen: 0000-0003-4645-6161

Xiao-Jun Su: 0000-0002-4060-0962

Jonah W. Jurss: 0000-0002-2780-3415

### Notes

The authors declare no competing financial interest.

## ■ ACKNOWLEDGMENTS

Acknowledgment is made to the donors of The American Chemical Society Petroleum Research Fund for support of this research (grant no. 58707-DNI3).

## ■ REFERENCES

- (1) Lindhorst, A. C.; Haslinger, S.; Kühn, F. E. Molecular iron complexes as catalysts for selective C–H bond oxygenation reactions. *Chem. Commun.* **2015**, *51*, 17193–17212.
- (2) Chen, K.; Costas, M.; Kim, J.; Tipton, A. K.; Que, L., Jr. Olefin *cis*-Dihydroxylation versus Epoxidation by Non-Heme Iron Catalysts: Two Faces of an Fe<sup>III</sup>-OOH Coin. *J. Am. Chem. Soc.* **2002**, *124*, 3026–3035.
- (3) Bae, S. H.; Seo, M. S.; Lee, Y.-M.; Cho, K.-B.; Kim, W.-S.; Nam, W. Mononuclear nonheme high-spin (*S* = 2) versus intermediate-spin (*S* = 1) iron(IV)-oxo complexes in oxidation reactions. *Angew. Chem., Int. Ed.* **2016**, *55*, 8027–8031.
- (4) Nam, W.; Lee, Y.-M.; Fukuzumi, S. Tuning reactivity and mechanism in oxidation reactions by mononuclear nonheme iron(IV)-oxo complexes. *Acc. Chem. Res.* **2014**, *47*, 1146–1154.
- (5) Nam, W. High-valent iron(IV)-oxo complexes of heme and non-heme ligands in oxygenation reactions. *Acc. Chem. Res.* **2007**, *40*, 522–531.
- (6) Seo, M. S.; Kim, N. H.; Cho, K.-B.; So, J. E.; Park, S. K.; Clémancey, M.; Garcia-Serres, R.; Latour, J.-M.; Shaik, S.; Nam, W. A mononuclear nonheme iron(IV)-oxo complex which is more reactive than cytochrome P450 model compound I. *Chem. Sci.* **2011**, *2*, 1039–1045.

- (7) Chen, M. S.; White, M. C. A predictably selective aliphatic C-H oxidation reaction for complex molecule synthesis. *Science* **2007**, *318*, 783–787.
- (8) England, J.; Gondhia, R.; Bigorra-Lopez, L.; Petersen, A. R.; White, A. J. P.; Britovsek, G. J. P. Towards robust alkane oxidation catalysts: electronic variations in non-heme iron(II) complexes and their effect in catalytic alkane oxidation. *Dalton Trans* **2009**, *27*, 5319–5334.
- (9) Nehru, K.; Seo, M. S.; Kim, J.; Nam, W. Oxidative N-dealkylation reactions by oxoiron(IV) complexes of nonheme and heme ligands. *Inorg. Chem.* **2007**, *46*, 293–298.
- (10) Grau, M.; Kyriacou, A.; Martinez, F. C.; de Wispelaere, I. M.; White, A. J. P.; Britovsek, G. J. P. Unraveling the origins of catalyst degradation in non-heme iron-based alkane oxidation. *Dalton Trans* **2014**, *43*, 17108–17119.
- (11) (a) England, J.; Martinho, M.; Farquhar, E. R.; Frisch, J. R.; Bominaar, E. L.; Münck, E.; Que, L., Jr. A synthetic high-spin oxoiron(IV) complex: generation, spectroscopic characterization, and reactivity. *Angew. Chem., Int. Ed.* **2009**, *48*, 3622–3626. (b) Bigi, J. P.; Harman, W. H.; Lassalle-Kaiser, B.; Robles, D. M.; Stich, T. A.; Yano, J.; Britt, R. D.; Chang, C. J. A high-spin iron(IV)-oxo complex supported by a trigonal nonheme pyrrolide platform. *J. Am. Chem. Soc.* **2012**, *134*, 1536–1542.
- (12) Draksharapu, A.; Li, Q.; Logtenberg, H.; van den Berg, T. A.; Meetsma, A.; Killeen, J. S.; Feringa, B. L.; Hage, R.; Roelfes, G.; Browne, W. R. Ligand exchange and spin state equilibria of  $\text{Fe}^{\text{II}}(\text{N4Py})$  and related complexes in aqueous media. *Inorg. Chem.* **2012**, *51*, 900–913.
- (13) England, J.; Britovsek, G. J. P.; Rabadia, N.; White, A. J. P. Ligand topology variations and the importance of ligand field strength in non-heme iron catalyzed oxidations of alkanes. *Inorg. Chem.* **2007**, *46*, 3752–3767.
- (14) (a) Chen, K.; Que, L., Jr. Stereospecific alkane hydroxylation by non-heme iron catalysts: mechanistic evidence for an  $\text{Fe}^{\text{V}}=\text{O}$  active species. *J. Am. Chem. Soc.* **2001**, *123*, 6327–6337. (b) Hong, S.; Lee, Y.-M.; Cho, K.-B.; Sundaravel, K.; Cho, J.; Kim, M. J.; Shin, W.; Nam, W. Ligand topology effect on the reactivity of a mononuclear nonheme iron(IV)-oxo complexes in oxygenation reactions. *J. Am. Chem. Soc.* **2011**, *133*, 11876–11879.
- (15) (a) Que, L., Jr.; Tolman, W. B. Biologically inspired oxidation catalysis. *Nature* **2008**, *455*, 333–340. (b) Bryliakov, K. P.; Talsi, E. P. Active sites and mechanisms of bioinspired oxidation with  $\text{H}_2\text{O}_2$ , catalyzed by non-heme Fe and related Mn complexes. *Coord. Chem. Rev.* **2014**, *276*, 73–96.
- (16) Khnayzer, R. S.; Thoi, V. S.; Nippe, M.; King, A. E.; Jurss, J. W.; El Roz, K. A.; Long, J. R.; Chang, C. J.; Castellano, F. N. Towards a comprehensive understanding of visible-light photogeneration of hydrogen from water using cobalt(II) polypyridyl catalysts. *Energy Environ. Sci.* **2014**, *7*, 1477–1488.
- (17) McDonald, A. R.; Que, L., Jr. High-valent nonheme iron-oxo complexes: Synthesis, structure, and spectroscopy. *Coord. Chem. Rev.* **2013**, *257*, 414–428.
- (18) Bigi, J. P.; Hanna, T. E.; Harman, W. H.; Chang, A.; Chang, C. J. Electrocatalytic reduction of protons to hydrogen by a water-compatible cobalt polypyridyl platform. *Chem. Commun.* **2010**, *46*, 958–960.
- (19) Hitomi, Y.; Arakawa, K.; Funabiki, T.; Kodera, M. An iron(III)-monoamidate complex catalyst for selective hydroxylation of alkane C-H bonds with hydrogen peroxide. *Angew. Chem., Int. Ed.* **2012**, *51*, 3448–3452.
- (20) Groves, J. T.; Nemo, T. E. Aliphatic hydroxylation catalyzed by iron porphyrin complexes. *J. Am. Chem. Soc.* **1983**, *105*, 6243–6248.
- (21) Ghosh, M.; Pattanayak, S.; Dhar, B. B.; Singh, K. K.; Panda, C.; Gupta, S. S. Selective C–H bond oxidation catalyzed by the Fe-bTAML complex: Mechanistic implications. *Inorg. Chem.* **2017**, *56*, 10852–10860.
- (22) Company, A.; Gómez, L.; Güell, M.; Ribas, X.; Luis, J. M.; Que, L., Jr.; Costas, M. Alkane hydroxylation by a nonheme iron catalyst that challenges the heme paradigm for oxygenase action. *J. Am. Chem. Soc.* **2007**, *129*, 15766–15767.
- (23) Klopstra, M.; Roelfes, G.; Hage, R.; Kellogg, R. M.; Feringa, B. L. Non-heme iron complexes for stereoselective oxidation: Tuning of the selectivity in dihydroxylation using different solvents. *Eur. J. Inorg. Chem.* **2004**, *2004*, 846–856.
- (24) Comba, P.; Maurer, M.; Vadivelu, P. Oxidation of cyclohexane by high-valent iron bispidine complexes: Tetradentate versus pentadentate ligands. *Inorg. Chem.* **2009**, *48*, 10389–10396.
- (25) Nagataki, T.; Tachi, Y.; Itoh, S. Synthesis, characterization, and catalytic oxygenation activity of dinuclear iron(III) complex supported by binaphthol-containing chiral ligand. *J. Mol. Catal. A: Chem.* **2005**, *225*, 103–109.
- (26) Costas, M.; Chen, K.; Que, L., Jr. Biomimetic nonheme iron catalysts for alkane hydroxylation. *Coord. Chem. Rev.* **2000**, *200*–202, 517–544.